Extended Abstracts of the 2017 International Conference on Solid State Devices and Materials, Sendai, 2017, pp149-150

C-5-04

CMOS compatible 200mm silicon photonic platform suitable for high bandwidth applications

B. Szelag [1], B.Charbonnier[1], S. Brision[1], B. Karakus[1], D. Fowler[1], O. Lemonnier[1], J.M. Hartmann[1], P. Brianceau[1], D. Marris-Morini[2], E. Cassan[2], L. Vivien [2], S. Menezo[1], C. Kopp[1]

[1] University Grenoble Alpes and CEA, LETI, Minatec Campus, F-38054 Grenoble Cedex, France.
[2] Centre de Nanosciences et Nanotechnologies (C2N), Univ. Paris Sud, Univ. Paris SAclay, Orsay, France
bertrand.szelag@cea.fr

Abstract

A 200mm silicon photonics platform supported by a PDK is presented. An advanced silicon patterning module is used. Recent advances in High-speed photodetectors and modulators integrated in SOI platform are reported and applied for photonic applications.

1. Introduction

Silicon photonics is becoming a technology of choice for optical communications. Compatibility with CMOS manufacturing process is one key of success since it allows taking advantage of the production capacities of foundries; i.e. large volume and low cost manufacturability [1-2]. The integration of high performance devices is the major outcome to achieve for these platforms. In this paper, we present a 200mm silicon photonics platform with state of the art devices suitable for high bandwidth applications.

2. Process Overview and Passive devices

A modular approach is used to build the process flow that supports various sets of devices. Fig.1 illustrates the process integration scheme. Starting material are Silicon-On-Insulator substrates with 310nm thick silicon films on top of 800nm thick BOX; handling wafers use high resistivity silicon. A multi-level silicon patterning module allows the fabrication of waveguides with different slab heights, leading to different optical characteristics, which can be mixed inside the same die. Deep Ultra Violet 193nm lithography is used for the most critical levels. Linear transmission loss for each type of device has been extracted as well as the minimum radius for lossless bends. Results are presented in the table of Fig.2. The patterning module is also used to fabricate the surface grating couplers with no dedicated masks. Fig. 3 shows a tilted Scanning Electron Microscopy picture of 1D and 2D grating couplers. Fig. 4 presents the optical performances of these coupling devices. The typical coupling loss of Single Polarization Grating Couplers (SPGC) in the O-band (1260-1360nm) is 2.0dB with a -1dB bandwidth of 26nm and a back reflection below -20 dB. Polarization diversity grating couplers (PSGC) have insertion losses lower than 4dB with a -1dB bandwidth of 24nm and a typical polarization dependent loss less than 0.5dB. The process design kit (PDK) supporting this platform proposes a device library containing a large set of passive devices such as Multi-Mode-Interferometer, MUX/deMUX or waveguide transitions and crossings for instance.

3. Active devices

Photodetector (PD) is a key device for most of the photonic integrated circuit in particular as receiver or monitoring device within transceiver circuit. Selective epitaxial groth of Germanium is used to absorb the light [2]. A new waveguide photodetector based on a double hetero-structure SiGeSi has been developed (see Fig.5) leading to a better light confinement compared to full-Ge device and higher responsivity. Moreover, this structure is compatible with silicided contacts, which improves the access resistance and reduces the technological process. Fig. 6 and 7 show SEM views of the detector during the fabrication. Fig 8, 9 and 10 report on the main characteristics of the device at a wavelength of 1310nm. Responsivity as high as 1A/W and bandwidth higher than 30GHz were achieved. A clear open eye diagram at. 30 Gb/s has been demonstrated (Fig. 11).

The second key component is the Mach Zenhder Modulator (MZM). We have then designed a MZM to operate at 1310nm with low insertion loss (IL). Fig 12 shows a cross-section of a linear junction device. The targeted doping concentrations of the junction were 5.10^{17} cm^{-3} and 8.10^{17} cm^{-3} for the holes and the electrons, respectively. Fig 13 shows a tilted SEM picture of the Mach-Zenhder Interferometer (MZI) modulator. A thin slab is used to improve the light confinement within the device. Fig. 14 illustrates the behavior of the MZM under DC bias. An average modulation efficiency ($V\pi L\pi$) of 1.9V.cm at 2.5V is obtained on 78 modulators of the same type, insertion loss being 6.5 dB/cm. Device's modulation capabilities are illustrated by various eye diagrams captured for a 3mm long MZM at 32Gbps NRZ (Fig15), 52Gbps NRZ (Fig16) and 28GBaud PAM4 (Fig17). For these modulation demonstration, MZM have been used in single drive configuration. The MZM are designed to operate in push-pull mode and a higher extinction ratio is expected.

4. Conclusions

A CMOS process compatible with silicon photonic platform has been developed. Advanced silicon patterning module allows the design of advanced passive devices. Integrated photodetectors and modulators have demonstrated high-speed capabilities together with state of the art optical characteristics. This platform is suitable for high bandwidth circuits in the field of telecom and datacenter applications.

References

[1] F.Boeuf et al, Proc. IEDM, (2013), pp353-356
[2] N. B. Feilchenfeld et al, Proc. IEDM, (2015), pp652-655
[3] L. Vivien et al, Opt. Express, pp.6252–7, Apr. 2009.

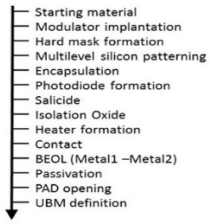

Fig. 1: Process integration scheme

Wave Guide type	Nominal width	Typical Linear Loss	Critical Radius
Single Mode Shallow Rib	400 nm	1.5 dB/cm	20 µm
Multimode Shallow Rib	1.8 µm	0.15 dB/cm	na
Single Mode Deep Rib	350 nm	3.5 dB/cm	4 µm
Single Mode Strip	350 nm	3.5 dB/cm	3 µm

Fig. 2: Waveguide basic characteristics at 1310nm. Typical linear loss and critical radius measured for each type of waveguide structures.

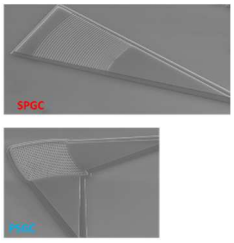

Fig. 3: Grating couplers SEM views

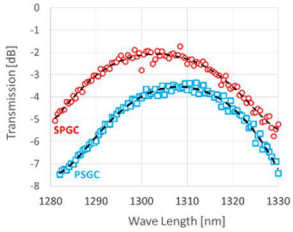

Fig 4: Transmission at 1310nm of 1D and 2D grating couplers

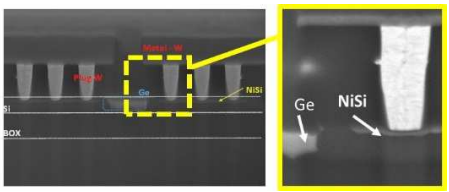

Fig. 5: Final cross section SEM view of a Si/Ge/Si architecture photodiode with zoomed view of a W-plug landing on silicided doped Si.

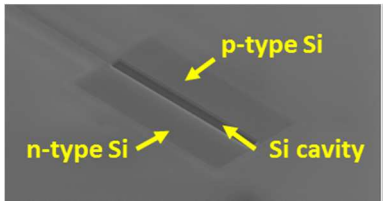

Fig. 6: Tilted SEM image of the silicon cavity surrounded by doped silicon regions

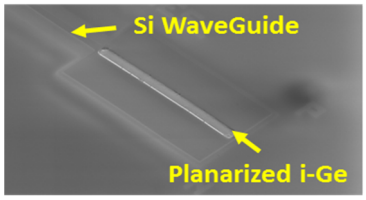

Fig. 7: Tilted SEM image of the photodiode after germanium CMP showing the Butt coupled silicon waveguide.

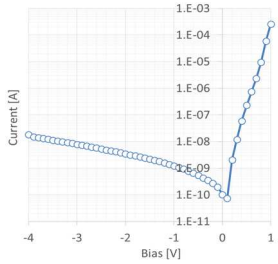

Fig. 8: I(V) characteristics of the Si/Ge/Si PhotoDetector (PD).

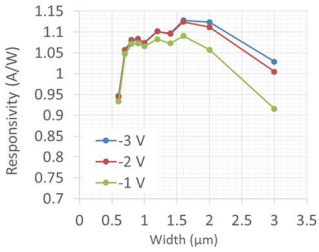

Fig. 9: PD Responsivity at 1310 nm vs. cavity width for various bias.

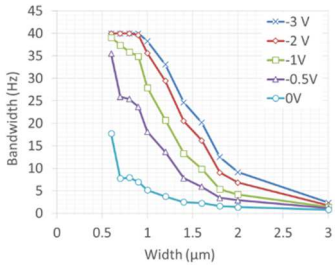

Fig. 10: PD 3dB RF Bandwidth vs. cavity width for various bias.

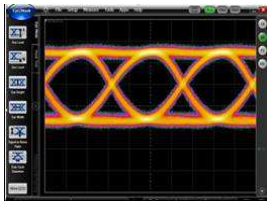

Fig. 11: 0.8µm wide SiGeSi photodiode eye diagram at 30Gb/s

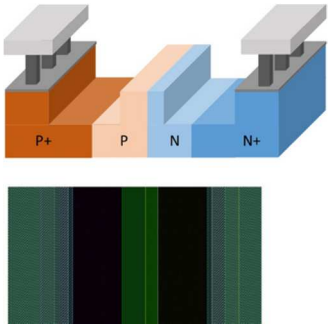

Fig. 12: MZM modulator cross-section and layout for linear junction based device.

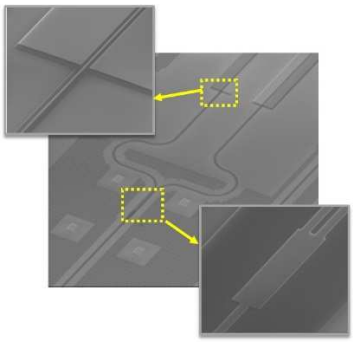

Fig. 13: SEM images of MZI modulators. P doped regions of each arm are facing each other. A 1x2 MMI is used at the input.

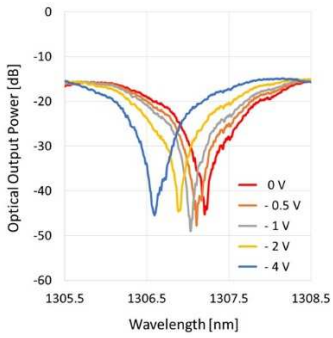

Fig. 14: Response spectra of a 3mm-long MZI modulator at different voltages

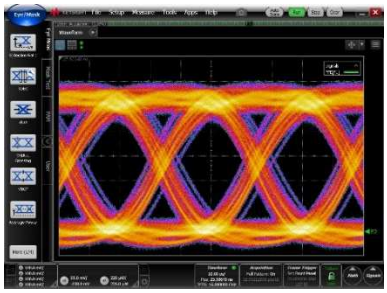

Fig. 15: 3mm long MZI Modulator 32Gbps NRZ eye diagram

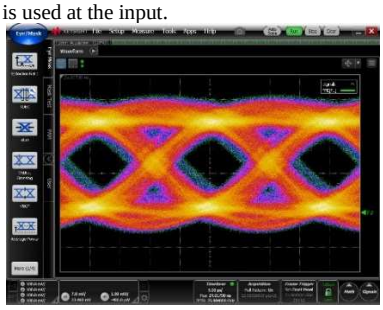

Fig. 16: 3mm long MZI Modulator 52Gbps NRZ eye diagram

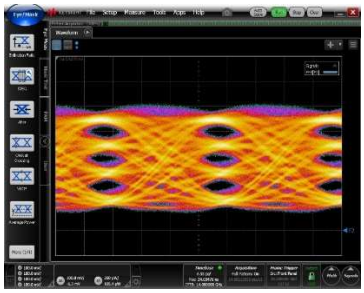

Fig. 17: 3mm long MZI Modulator 28GBaud PAM4 eye (after CTLE 4dB applied and using de-emphasis on the TX side